The Influence of Composition and Processing Parameters on the Mechanical Properties and Erosion Response of Ni + TiB$_2$ Coatings

James J. Wert and Scott J. Oppliger

Sputtered Ni + TiB$_2$ coatings have been shown to protect Inconel* 718 and Ti-6Al-4V substrates from solid particle erosion. However, before new erosion-resistant coatings can be efficiently designed, it is essential that the role of mechanical properties in determining erosion resistance be fully understood. In this investigation, nanoindentation techniques were used to quantify the effects of substrate preparation, coating composition, and sputtering process parameters on the elastic moduli and indentation hardness of thin coatings deposited on Ti-6Al-4V and Inconel 718 substrates. The influence of these parameters on coating adhesion was determined using a conventional scratch test. Elastic moduli, indentation hardnesses, and coating adhesion were correlated with erosion behavior. The erosion resistance of those coatings that exhibited microscopic ductility is dependent on the nodule diameter and coating properties such as hardness, elastic modulus, and fracture toughness.

1 Introduction

SOLID particle erosion is the response of a material to impact by a particle carried in a fluid stream and is generally measured and reported as a mass loss of target material per impacting mass of erodent particles, or more recently, as a volume of target material lost per impacting mass of erodent particles. Structural components for many energy conversion devices are often susceptible to erosion due to interaction with particles entrained in either gases or liquids. For example, an important problem in air transportation is the erosion of compressor blades in gas turbine engines. The effects of erosion are observed as a loss of power, loss of surge margin, and increased fuel consumption. Other examples include the limitations on useful operating lifetimes of coal gasification plants and slurry pipelines due to the lack of erosion resistance of various valves, seals, bearings, and fittings.

The erosion response of a material is a complex function of the physical and mechanical properties of the target and particle materials and the parameters defining the erosive environment. According to Finnie,[1] there are four major factors that influence the erosion response of any particular system. These factors are the particle velocity, angle of impingement, particle properties, and the properties of the material being eroded. The impingement angle is the angle between the target surface and the particle trajectory. Ductile materials exhibit maximum erosion for glancing impacts (*i.e.*, generally between 15 and 30°), whereas brittle materials exhibit their maximum erosion rates at normal impingement angles.

In many applications, the system requirements dictate the mechanical properties of the alloy and leave little opportunity for alloy optimization. Therefore, during the past several decades, the use of thin coatings to protect metallic substrates from

attack by erosive environments has achieved increased importance. However, before new erosion-resistant coatings can be efficiently designed, it is essential that the role of mechanical properties, such as elastic modulus, indentation hardness, and fracture toughness, in determining erosion behavior be fully understood.

The mechanical properties of bulk materials have been used to predict their erosion behavior. For example, Ruff and Wiederhorn[2] have obtained an expression for the erosion of brittle materials by modifying the erosion model developed by Evans *et al.*[3] for material removal by single impacts. Although several semiempirical terms were required to adequately describe erosion due to multiparticle impacts, the erosion rate was found to be inversely proportional to the critical stress-intensity factor, K_c, and directly proportional to the indentation hardness, H, as shown in the equation below:

$$w = V_o^{2.4} R^{3.7} \rho^{1.2} K_c^{-1.3} H^{0.11} \qquad [1]$$

where w is the volume of material removed, V_o is the impacting particle velocity, ρ is particle density, and R is particle radius.

The erosion process in most brittle coatings is similar to that observed in brittle bulk materials in that the particle impacts induce the formation of cracks at or below the surface, followed by crack propagation or growth. The erosion process can be greatly accelerated by the presence of defects that lead to the formation of pinholes.[4, 5] Pinholes are erosion craters in which substrate material has been exposed. Many coatings also spall when exposed to erosion due to a lack of adhesion between the coating and the substrate. According to Thornton,[6] depending on the ratio of T/T_m and the sputtering gas pressure, it is possible to form the four different coating morphologies shown in Fig. 1.[7] In this expression, T is the temperature of the substrate, and T_m is the melting point of the coating material in degrees Kelvin.

Chopra[8] has found that the microindentation hardness of sputtered Al films doped with Al$_2$O$_3$ demonstrated a strong dependence of hardness on the deposition rate. He also found that increasing the substrate temperature during sputtering de-

James J. Wert, George A. Sloan Professor of Metallurgy, Department of Materials Science & Engineering, Vanderbilt University; and **Scott J. Oppliger**, Department of Materials Science & Engineering, Vanderbilt University, Nashville, Tennessee.
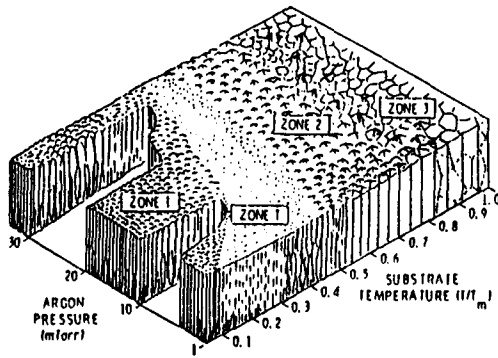*Inconel 718 is a trademark of The International Nickel Co.

Fig. 1 Schematic diagram of the coating growth morphology as a function of substrate temperature and argon working gas pressure. T is the substrate temperature, and T_m is the melting point of the coating material in degrees Kelvin.[7]
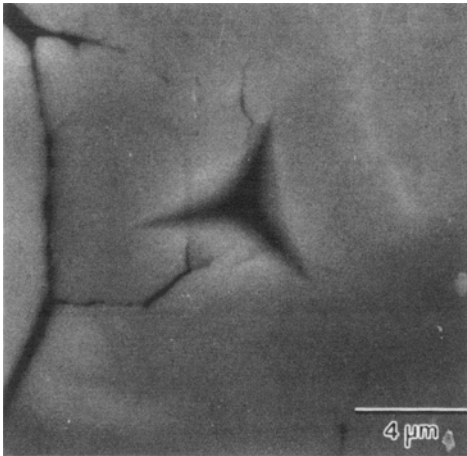

Fig. 3 Typical load vs. displacement curve obtained from the Nanoindenter.[9]

Fig. 2 Scanning electron micrograph of a typical plastic impression produced by the triangular pyramidal indenter used in the Nanoindenter.[9]

creased the hardness of the film markedly. Because the erosion behavior of bulk materials is related to their mechanical properties, it is expected that a relationship similar to Eq 1 might be applicable to coated systems.

The mechanical properties of a coating are a reflection of its microstructure. Therefore, to obtain a detailed understanding of the influence of composition and processing parameters on erosion resistance, their influence on the resulting microstructures and mechanical properties of the coating must be identified.

Both Vickers and Knoop microindentation hardness tests have been used to obtain a measure of the mechanical properties of thin coatings. However, because many erosion-resistant coatings are very thin and also brittle, very light loads must be used to prevent penetration and fracture of the coating. Therefore, traditional microindentation methods are not feasible. To avoid fracture of the coating and substrate effects, extremely small and precise loads must be applied. In a previous paper,[9] it was shown that a nanoindentation technique developed by Oliver et al.[10] could be used to compare the elastic moduli and hardnesses of very thin coatings.
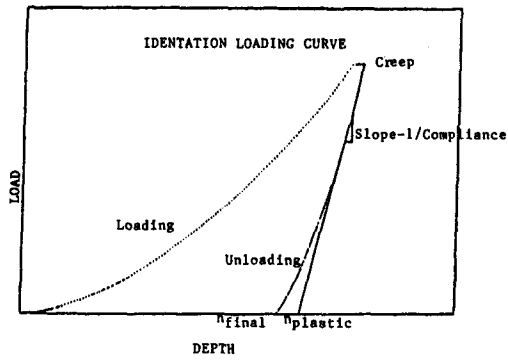
The Nanoindenter* is a depth- and load-sensing instrument that is programmed to load and unload a diamond indenter at a constant rate. A scanning electron micrograph (SEM) of a typical impression created by the indenter in $10Ni + TiB_2$ is shown in Fig. 2. A load-displacement curve showing the difference between the plastic depth (h_p) and final depth(h_f), and the slope, S, of the first one third of the unloading curve is shown in Fig. 3.

The slope of the unloading curve can be used to obtain the elastic properties of a sample material. Doerner and Nix[11] have modified a solution of Sneddon[12] for bulk materials to calculate the Young's modulus of thin coatings:

$$1/E_r = (1 - v_D^2)/E_D + (1 - v_o^2)E_o \qquad [2]$$

where E_r is the composite Young's modulus of the system, E_D is Young's modulus of diamond, E_o is Young's modulus of the coating, v_D is Poisson's ratio of diamond, and is Poisson's ratio of the coating.

The reciprocal slope, dh/dP, during the initial unloading curve for an ideal triangular pyramidal indenter is related to the compliance of a material. Because the compliance is the inverse of the stiffness, S, it may be shown that:

$$dh/dP = 1/S - 1/h_p \times 1/E_r = \frac{1}{h_p E_r} \qquad [3]$$

where h_p is the plastic depth. Assuming that the composite modulus is proportional to the stiffness, S, divided by the square root of the projected area, A, in contact with the indenter:

$$E_r \approx S/A^{1/2} \qquad [4]$$

where S is the slope determined by linear regression analysis of the first one-third of the unloading curve shown in Fig. 3. The projected area of contact, A, can be obtained from:

$$A = k_1 h_p^2 + k_2 h_p^{1.5} + k_3 h_p \qquad [5]$$

---

*Nanoindenter is a commercial tradename.

Table 1 Sputter Coating Process Parameters

Coating number	Deposition rate, Å/min	Bias voltage, V	Sputter cleaning, min	Substrate surface preparation	Coating composition, wt%
1	2400	100	15	W	$10Ni(TiB_2)$
2	2400	25	15	X	$10Ni(TiB_2)$
3	2400	25	30	W	$10Ni(TiB_2)$
4	2400	100	30	X	$10Ni(TiB_2)$
5	1500	100	30	Y	$10Ni(TiB_2 + 10MoB)$
6	1500	100	30	Y	$10Ni(TiB_2 + 10WC)$
7	1500	100	30	Y	$10Ni(TiB_2 + 10Cr_3C_2)$
8	2100	100	30	Z	$0Ni(TiB_2)$
9	2100	100	30	Z	$20Ni(TiB_2)$

Note: W ≡ grit blast, 180-grit Al_2O_3, 45 psi, 45°. X ≡ liquid vapor hone, 1250-grit Al_2O_3 in water, 80 psi, 45 to 60°. Y ≡ grit blast, 220-grit Al_2O_3 at 45°. Z ≡ grit blast, 220-grit Al_2O_3 at 60°.
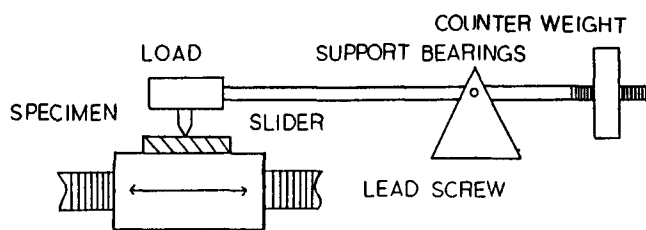
Fig. 4 Schematic diagram of the scratch test apparatus.
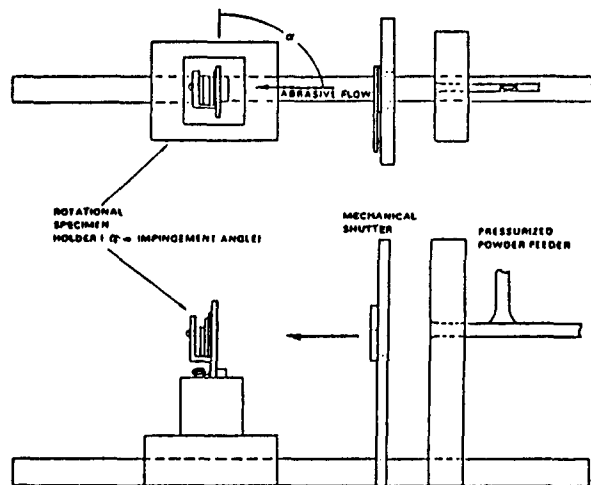
Fig. 5 Schematic diagram of erosion apparatus.

where k_1, k_2, and k_3 are, respectively, the geometric shape factor constants for the pyramidal diamond indenter. Because h_p cannot be determined with great accuracy, the area may be approximated by:

$$A \approx kh_p^2 \qquad [6]$$

where k is equal to 24.5.

Table 2 Erosion Test Conditions

Abrasive .... Pure alumina (Al_2O_3)
Density .... 3.99 g/cm^3
Size .... 85 ± 50 μm in diameter
Hardness .... ~15 GPa
Velocity .... 50 ± 3.5 m/sec

Erosion variables

Impingement angle .... 30 and 90°
Concentration .... 0.14 ± 0.02 and 0.32 ± 0.04 g/sec
Exposed area .... 0.71 cm^2
Nozzle length to diameter ratio 18:1

Environment

Carrier gas .... Nitrogen
Temperature .... Ambient
Gas pressure .... Carrier = 50 psi, feeder = 70 psi

Materials tested

Substrate materials
A Ti-6Al-4V
B .... Inconel 718
Coatings
A .... 1, 2, 3, 5, 6, 7, 8, and 9
B .... 1, 2, 3, 4, 5, 6, 7, 8, and 9

The hardness, H, of a material is related to the maximum applied load, P_{max}, divided by the projected area of contact, A:
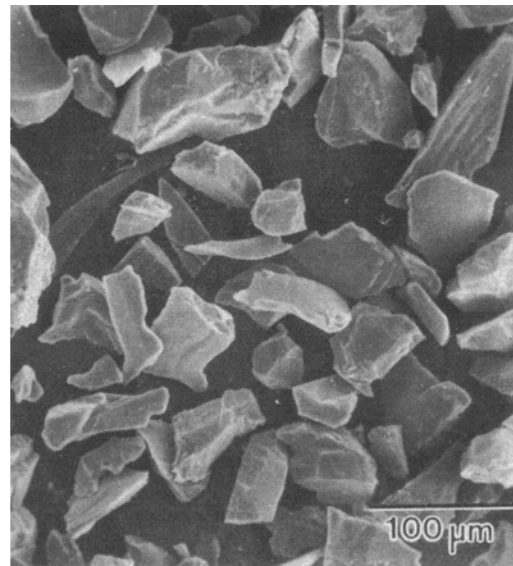
$$H \approx P_{max}/kh_p^2 \qquad [7]$$

which is the approximation used to obtain hardness values of thin coatings.

2 Experimental Procedure and Materials

The Ti-6Al-4V (substrate A) and Inconel 718 (substrate B) alloys used in this investigation were sputter coated by the Xytor
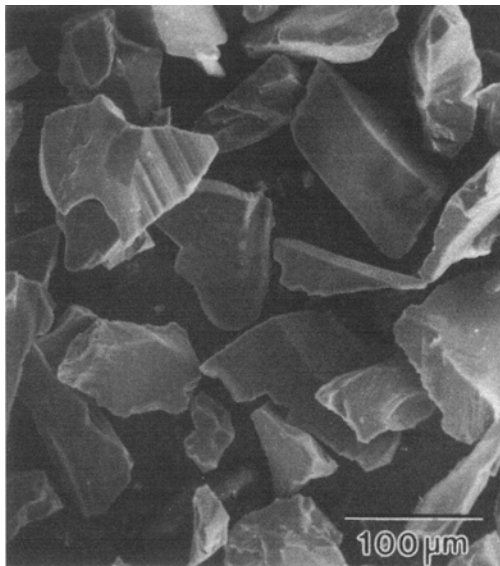
(a)

(b)

Fig. 6 (a) SEM micrograph of Al₂O₃ particles (85 ± 50 μm in diameter). (b) Worn Al₂O₃ particles (58 ± 31 μm in diameter).

Corporation. A planar high deposition rate, D.C. Magnetron, multiple-pass sputtering unit was used to apply 30-μm thick ceramic coatings on one side of each sample. As shown in Table 1, three different sets of samples were examined. Table 1 outlines the coating application process parameters, coating compositions, substrate preparation, and cleaning methods used. Although the first set of samples (*i.e.*, 1, 2, 3, 4A, and B) were all coated with 10Ni + TiB₂, different processing parameters were used to prepare the Ti-6Al-4V and Inconel substrates. For the second series of samples (*i.e.*, 5, 6, 7A, and B), the substrate preparation and processing parameters were identical and the composition of the coatings varied. The third set of samples (*i.e.*, 8, 9A, and 9B) was designed to allow examination of the role of the Ni binder in determining the erosion resistance of TiB₂.

The scratch tester shown in Fig. 4, equipped with a Brale diamond indenter, was used to obtain a relative measure of the adhesive strength between the coating and substrate. To obtain the minimum load necessary to cause delamination of the coating (*i.e.*, relative adhesive strength of the coating/substrate interface) normally required five to seven passes.

The mechanical properties of the coatings were determined using a Nanoindenter. Prior to testing, flat surfaces were obtained on the Nanoindenter samples by dimpling with a VCR Group dimpler using a flattening tool covered with billiard cloth immersed in 0.05-μm Al₂O₃ polishing compound. After mounting in bakelite, the samples were allowed to come to thermal equilibrium prior to testing. Ten indentations were made in each coating using the same loading/unloading sequence.

To determine the response of the coatings to solid particle impact, the coatings were tested at room temperature using the erosion conditions summarized in Table 2 and the erosion tester shown schematically in Fig. 5. The angular Al₂O₃ supplied by

S.S. White of Piscataway, New Jersey, is shown in Fig. 6 prior to and after an erosion test. Using the line intercept method, the diameters of the virgin and worn Al₂O₃ particles were found to be 85 ± 50 μm and 58 ± 31 μm, respectively. With dry nitrogen as the carrier and using the rotating disk method of Ruff and Ives,[13] the particle velocity was found to be 50 ± 3.5 m/sec. Because the abrasive stream has a near Gaussian particle density distribution, a thin rubber mask was used to shield the specimen surface so that a constant area of 0.71 cm² was exposed to the abrasive stream. This method allowed a constant particle concentration of 0.32 g/sec at an impingement angle of 90° and 0.14 g/sec at 30°. Prior to and after each exposure to the abrasive stream, the samples were ultrasonically cleaned in acetone and weighed to 0.01 mg. The erosion rates were expressed as milligrams of sample mass loss per gram of impacting Al₂O₃. The samples were eroded for periods of 10 to 270 sec. However, many tests had to be terminated after 10 to 20 sec due to catastrophic failure of the coating.

To determine the mechanism of erosion for each coating, single-impact experiments were conducted at both 30 and 90° impingement angles. Coatings were eroded in both the as-sputtered condition and after smoothing of the surface using the dimpling technique outlined for preparation of the Nanoindenter samples. These samples were exposed to the erosive stream for periods of 0.5 to 5 sec.

The effects of varying process parameters on the coating morphology, thickness, nodule size and integrity, and the damage resulting from the erosion process were evaluated using scanning electron microscopy. The average nodule size or diameter was determined by the line intercept method applied to defect-free regions of the samples.
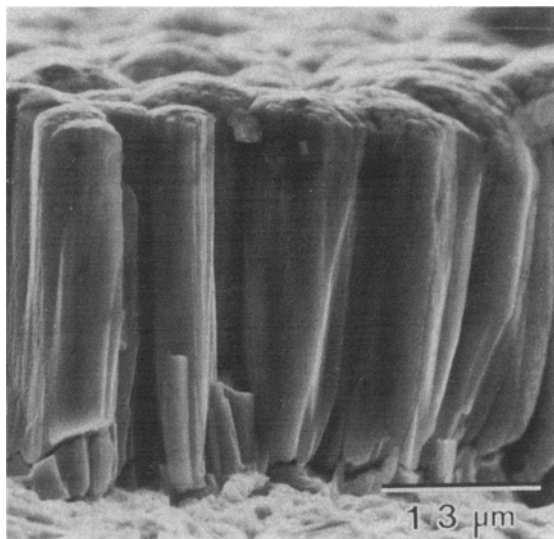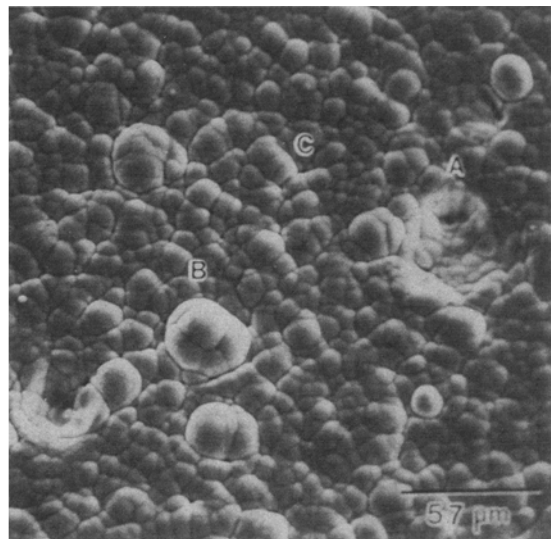
(a)   (b)

Fig. 7 (a) SEM micrograph of Coating 6, which possesses Zone 1-type growth morphology. (b) SEM micrograph of Coating 3, which illustrates typical coating defects: (**A**) craters, (**B**) kernels, and (**C**) voids.

Table 3 Nodule Diameter Characteristic of the Four Different Substrate Preparations

Substrate surface preparation process	Nodule diameter (a), μm
Grit blast with 180-grit Al_2O_3 at 45 psi and 45° angle	5.6 ± 0.4
Grit blast with 220-grit Al_2O_3 at 45° angle...........................	5.2 ± 0.6
Grit blast with 220-grit Al_2O_3 at 60° angle...........................	4.7 ± 0.1
Liquid vapor honed with water and 1250-grit Al_2O_3 at 80 psi and 45 to 60° angles..	3.0 ± 0.2

(a) These values were obtained by the line intercept method applied to SEM micrographs of defect-free portions of the coatings.

3 Experimental Results

3.1 *Microstructure*

Coatings 2 and 4 (*i.e.*, $10Ni + TiB_2$), deposited on substrates that had been liquid vapor honed, exhibited type T growth morphology, whereas all other surface preparations produced coatings with Zone 1-type growth morphology. The Zone 1 microstructure shown in Fig. 7 is illustrative of the growth morphologies of Coatings 1, 3, 5, 6, 7, 8, and 9 deposited on either Ti-6Al-4V or Inconel 718 substrates. The microstructure consists of tapered nodules with domed tops separated by boundaries containing voids. The average nodule size resulting from the different substrate preparation processes is shown in Table 3. Also shown in Fig. 7 are typical defects observed in sputtered coatings.

As shown in Fig. 8, the Zone T (transition) structure observed in Coatings 2 and 4 consists of a dense close-packed array of nodules with poorly defined boundaries. Such small nodules and narrow boundaries were only observed in coatings depos-

ited on substrates prepared by liquid vapor honing with 1250-grit Al_2O_3.

According to Thornton,[6] the Zone T structure is the limiting form of the Zone 1 structure at $T/T_m = 0$ on infinitely smooth substrates. Zone T structures have also been observed to form on relatively smooth substrates at T/T_m values that permit diffusion of sputtered atoms to overcome the nucleation effects caused by substrate roughness.[5, 14]

3.2 *Adhesion Tests*

A typical coating failure observed during scratch testing is shown in Fig. 9. The direction of sliding of the Brale indenter is from left to right. The amount of the coating removed is approximately three times the width of the contact diameter of the diamond indenter. The minimum loads to cause failure in a single pass of the slider are summarized in Table 4.

3.3 *Erosion Behavior*

To provide a basis for comparison of the efficacy of the different coatings and to allow determination of when the coating had been penetrated, the erosion behaviors of both Ti-6Al-4V and Inconel 718 were determined in the uncoated conditions at impingement angles of 30 and 90°. The data obtained are summarized in Table 5 in terms of both mass and volume loss. The volume losses were calculated using 4.45 g/cm^3 for the density of Ti-6Al-4V and 7.1 g/cm^3 for the density of Inconel 718. Because both substrates are ductile, the maximum erosion rates occurred at ~30°.

The erosion behavior of the various coatings at impingement angles of 30 and 90° are summarized in Table 6. Due to very poor adhesion, the $10Ni + TiB_2$ coating applied to the vapor-honed Ti-6Al-4V substrate failed during sample preparation and
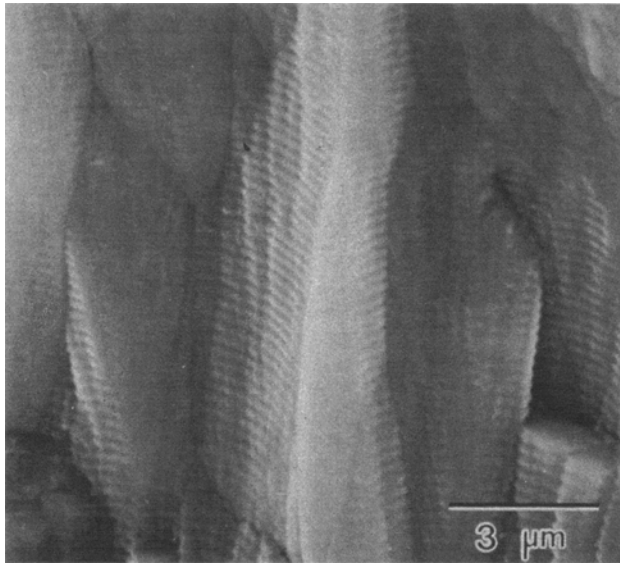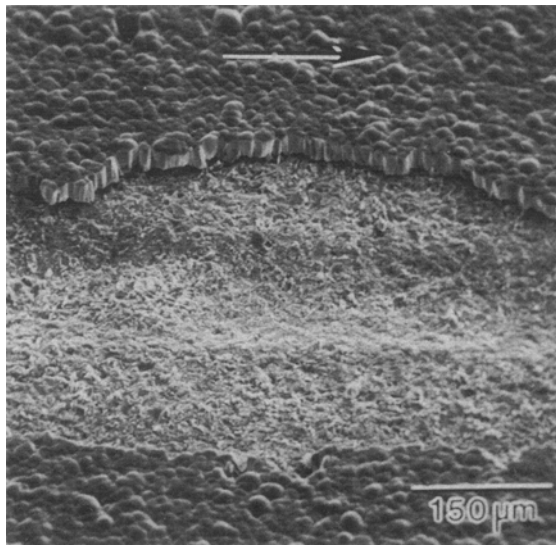
(a)
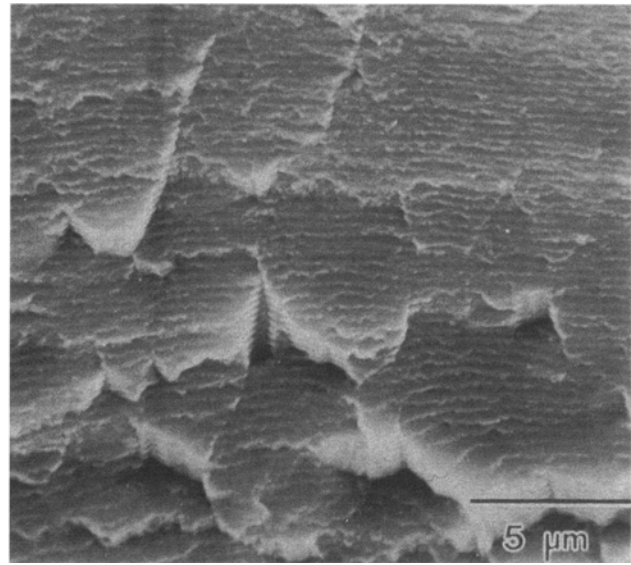
(b)

Fig. 8 Cross sections of Coating 4, which displays Zone T-type growth morphology. (a) Illustrates the competitive nature of the growth process. (b) Tapered cross section illustrating the close-packed nodule structure typical of coatings deposited on substrates that have been liquid vapor honed.

Fig. 9 Typical wear scar produced by the test.

could not be erosion tested. Coatings 1, 3, and 7 were not tested at 30° impingement angles due to their rapid failure at the 90° impingement angle. The initial erosion rates for these samples had to be estimated from:

$$w = 9.6 \text{ mg}/(0.32 \text{ g/sec})/t \text{ (sec)} \tag{8}$$

where 9.6 mg is the estimated coating mass removed by the erosive stream, which was obtained by multiplying the density of hot pressed TiB_2 (i.e., 4.5 g/cm^3) by the estimated volume loss.

Table 4 Scratch Test Results

Coating number	Load to cause failure ($\pm 20\%$), g
1A	4200
2A	5000
3A	4900
4A	3400
5A	4500
6A	6500
7A	3000
8A	3000
9A	3700
1B	4700
2B	4700
3B	4900
4B	4400
5B	4700
6B	4900
7B	2200
8B	5300
9B	3400

It is possible to classify the coatings into three groups in terms of their effectiveness as a barrier to substrate erosion:

- **Group I:** Coatings 1, 3, 7, and 9 exhibited rapid catastrophic failure and usually complete coating removal within 10 sec of exposure to the erosive stream.

- **Group II:** Coatings 5, 6, and 8 exhibited complete coating removal with exposure times of 40 to 90 sec. As shown in Fig. 10, the erosion rate is much higher at 90° impingement angles than at 30°.

- **Group III:** Coatings 2A, 2B, and 4B developed pinholes at coating defects. However, the pinholes did not grow catastrophically, and none of these samples suffered coating re-

moval even with extended exposure times of 270 sec. In addition, as shown in Fig. 11, Coatings 2B and 4B exhibited a ductile mode of erosion in that the erosion rate was higher at 30° than at 90°.

The erosion behavior described above was also reflected in the mode of material removal observed on a microscopic scale. The microstructure shown in Fig. 12 is illustrative of the initial erosion response of those coatings (i.e., 1, 3, 7, and 9) that failed catastrophically after very short exposure times. The initial impacts of the Al_2O_3 abrasive particles with these coatings resulted in brittle fracture of the columnar structure and removal of loosely bonded kernels. As shown in Fig. 13, erosion of Coatings 5 and 6 occurred via a combination of ductile plowing and brittle fracture. The increased ductility of these coatings resulted in the improved erosion resistance associated with the Group II coatings described previously.

The erosion behavior of the coatings classified as belonging to Group III (i.e., 2A, 2B, and 4B) is dramatically different from that observed for the other coatings. Although these coatings develop pinholes when exposed to an abrasive stream at a 30° impingement angle for 180 sec (Fig. 14), the pinhole walls erode in a ductile manner so that catastrophic failure never occurs. Similar behavior is observed at impingement angles of 90°. As shown in Fig. 15, after exposures of 270 sec, the coating surface and pinhole walls appear to be plastically deformed due to a ductile erosion process.
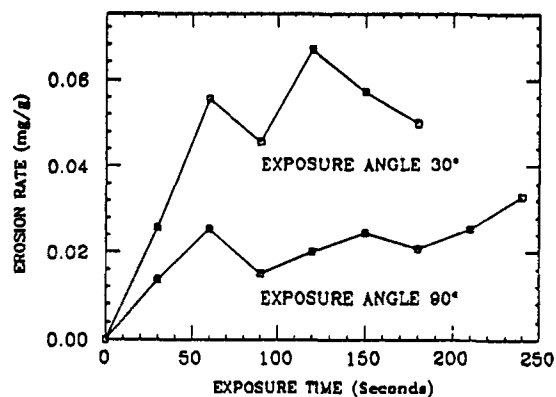
3.4 Mechanical Properties

To investigate the influence of substrate composition on the mechanical properties of sputtered coatings, the load-displacement curves shown in Fig. 16 for $10Ni(TiB_2 + 10MoB)$ deposited on Ti-6Al-4V and Inconel 718 were obtained. Using 2, 4, 6, and 7 and the data shown in Fig. 16, the elastic moduli and hardnesses of the coatings were found to be independent of the substrate. Therefore, further nanoindentation measurements were confined to only those coatings applied to Inconel 718 substrates. The data obtained are summarized in Table 7.

To minimize the effect of varying nodule size when evaluating the role of mechanical properties in determining the erosion response of nickel-bonded TiB_2 coatings, the hardnesses and

Table 6 Initial Erosion Rates of Coatings at Impingement Angles of 30 and 90°

| Coating number	Initial erosion rates, mg/g	
	$\alpha = 90°$	$\alpha = 30°$
1A	~6	...
2A	0.07 ± 0.06	0.08 ± 0.07
3A	~3 to 4	...
4A	(a)	(a)
5A	0.11 ± 0.06	...
6A	0.07 ± 0.05	0.01 ± 0.05
7A	~15	...
8A	0.76 ± 0.21	0.52 ± 0.13
9A	3.20 ± 0.62	0.21 ± 0.12
1B	~2 to 3	...
2B	0.01 ± 0.007	0.03 ± 0.01
3B	~1 to 3	...
4B	0.01 ± 0.003	0.03 ± 0.01
5B	0.09 ± 0.03	0.19 ± 0.09
6B	0.07 ± 0.02	0.12 ± 0.05
7B	~6 to 7	...
8B	0.43 ± 0.12	0.46 ± 0.09
9B	2.54 ± 0.91	0.13 ± 0.09

(a) Coating 4A could not be erosion tested due to delamination of the coating during specimen preparation.

Table 5 Erosion Rate of Substrate Material at 30 and 90° Impingement Angles Recorded in Mass Loss and Volume Loss per Impacting Mass or Erodant

Substrate material	Erosion rate	
	90° impingement	30° impingement
Ti-6Al-4V	0.48 ± 0.08 mg/g	1.10 ± 0.18 mg/g
	0.11 ± 0.02 cm³/g	0.25 ± 0.04 cm³/g
Inconel 718	0.70 ± 0.11 mg/g	1.35 ± 0.25 mg/g
	0.10 ± 0.02 cm³/g	0.19 ± 0.04 cm³/g
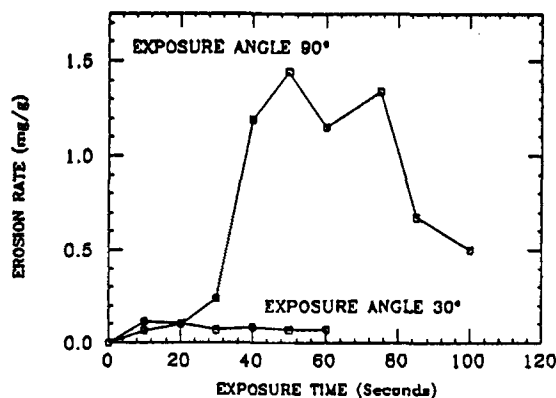
Fig. 10 Erosion rate vs exposure time at 30 and 90° impingement angles for Coating 6A.
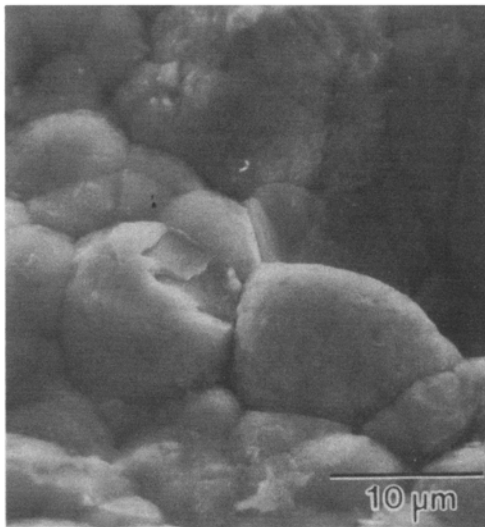

Fig. 11 Erosion rate vs exposure time at 30 and 90° impingement angles for coatings 2B and 4B.
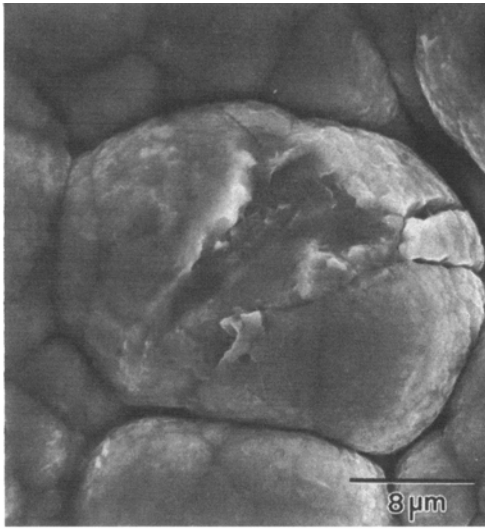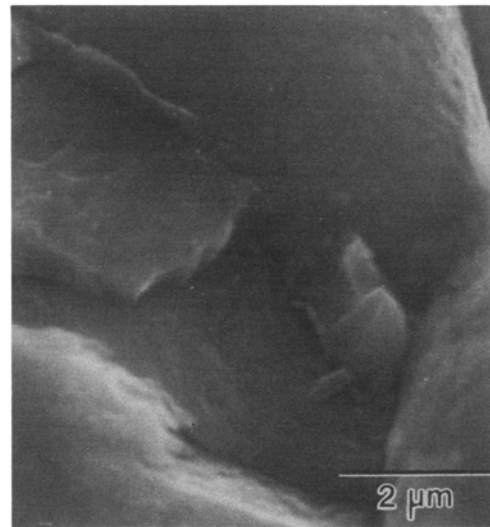
(a)
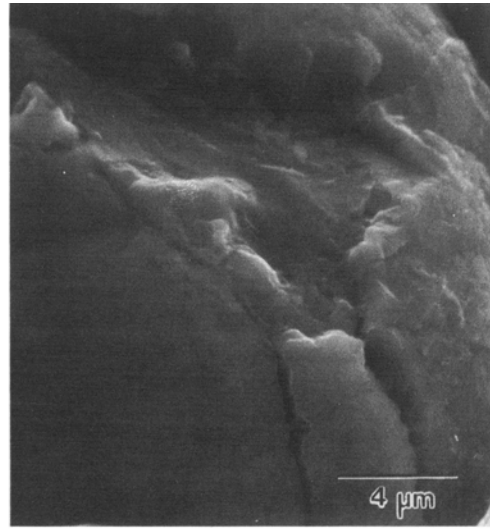
(b)

(c)

(d)

Fig. 12 Surface morphology of a brittle coating (*i.e.*, Coating 3) that has been eroded for 1 sec at a 90° impingement angle. (a) Brittle fracture of a kernel due to a single Al_2O_3 particle impact. (b) High magnification of the area in (a). (c) Fracture and plowing resulting from a single impact event. (d) High magnification of the area in (c).

elastic moduli were normalized with respect to nodule diameter. As shown in Fig. 17, for those coatings that did not fail catastrophically when exposed to an erosive stream (*i.e.*, 2, 4, 5, and 6B), the erosion resistance increased with increasing hardness, elastic modulus, and ultimate resiliency ($H^2/2E$). When the nodule size, d, is normalized to correct for the influence of hardness and elastic modulus (Fig. 18), the erosion rate was found to increase with increasing nodule size.
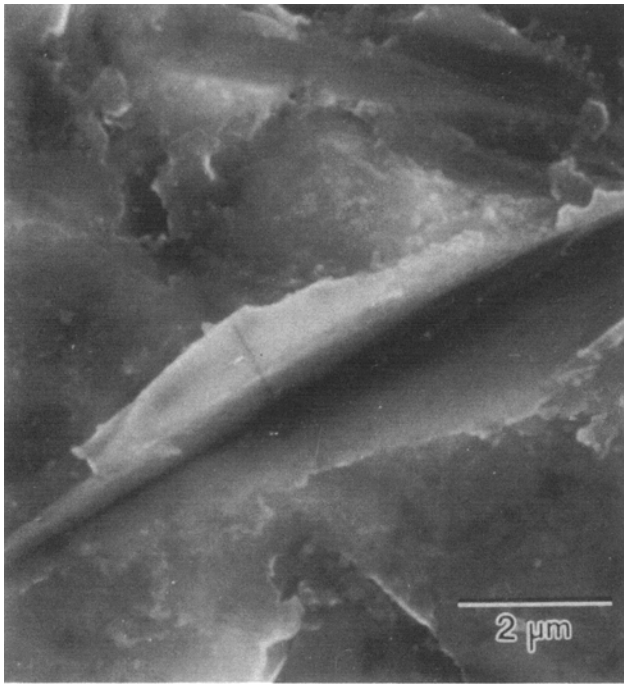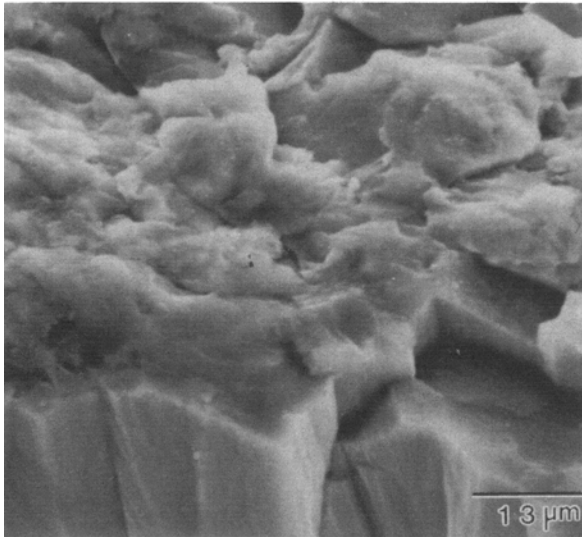
(a)
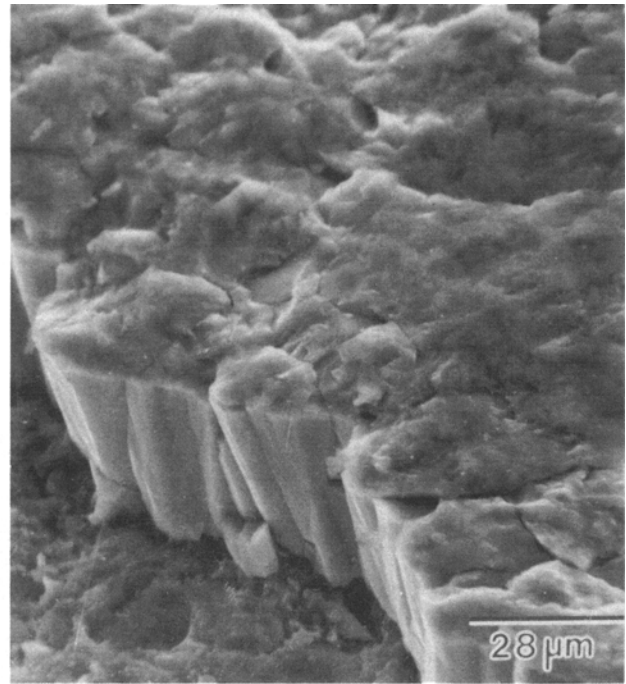
(b)

(c)

Fig. 13 Surface morphology of Coating 5 after erosion at 30 and 90° impingement angles. (**a**) Five-second exposure at 30° of a coated surface that had been polished smooth with a 0.5-μm Al_2O_3 slurry. Note ductility of the plowed lip. (**b**) Edge of an erosion pinhole after 10 sec at 90°. Note the extensive plastic deformation and chipping present. (**c**) Edge of an erosion pinhole illustrating fracture of the nodules that make up the pinhole wall and lateral crack surfaces present at the eroded surface.

4 Discussion

The Zone 1 structure that forms at low T/T_m is promoted by increased sputtering gas pressure, whereas the nodule diameter in Zone 1 increases with increasing T/T_m. In addition, sputtered coatings nucleate preferentially at substrate inhomogeneities. Because all of the coatings were applied at low T/T_m, the substrate surface roughness should determine the final growth structure and nodule diameter. Therefore, as shown in Table 3, the nodule diameter increases with increasing size of the grit
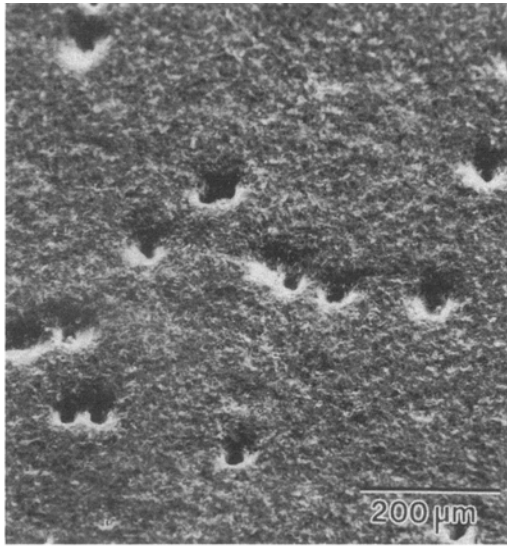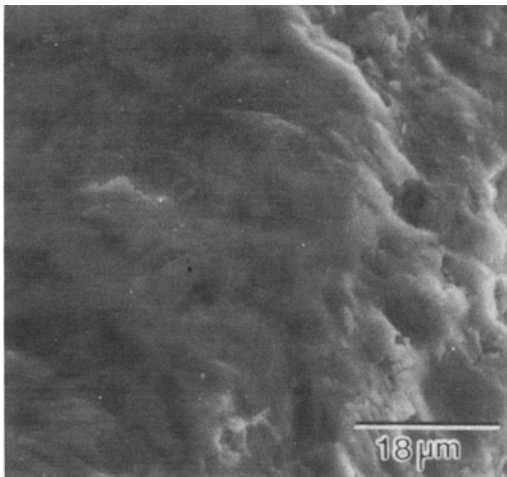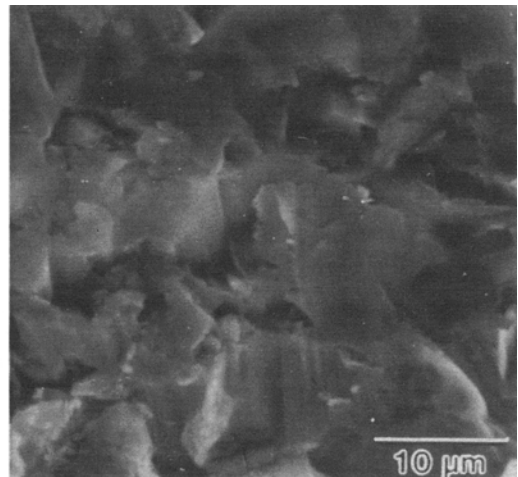
(a)
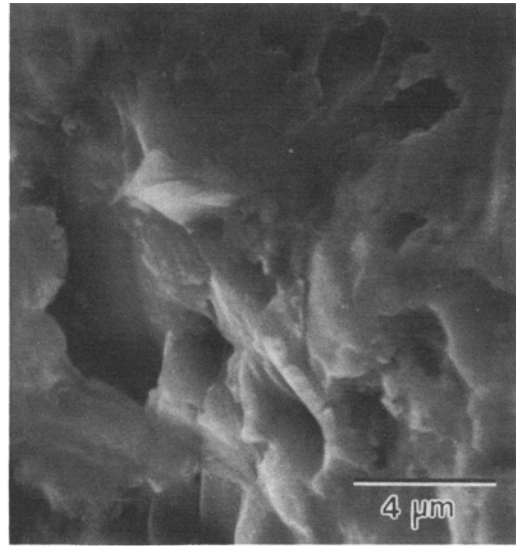
(b)

Fig. 14 Surface morphology of Coating 2A eroded for 180 sec at 30°. (a) Illustrates the formation of erosion pinholes at coating defects. (b) High magnification view of an erosion pinhole in (a) illustrating the ductile erosion process of pinhole walls.

(a)

(b)

Fig. 15 Surface morphology of Coating 2 eroded for 270 sec at 90°. (a) Illustrates the plastic deformation of the surface due to the impacting particles, which creates a smooth surface finish. (b) Illustrates the ductile erosion process at the walls of an erosion pinhole.

used to prepare the surface and, hence, reflects the substrate surface roughness.

The Group I coatings (*i.e.*, 1, 3, 7, and 9) failed almost immediately in a catastrophic manner due to spalling. The spalling resulted from the impact fracture extending down to the substrate/coating interface. The morphology of these coatings is quite similar and consists of large, non-close-packed nodules with a high incidence of voids and other defects. These sputter-coated surfaces are very rough. Therefore, single impacts by

Al_2O_3 (Fig. 12) causes devastating fracture and chipping of the coating.

The Group II (*i.e.*, 5, 6, and 8) coatings are appreciably more resistant to erosion than the Group I coatings due to the increased ductility available on the microscopic scale. In this group, the ductility is sufficient to allow plastic deformation and smoothing of the sputter-coated surface. The residual stresses resulting from plastic deformation of the surface during erosion initiate and drive lateral cracks, which form erosion chips (Fig.

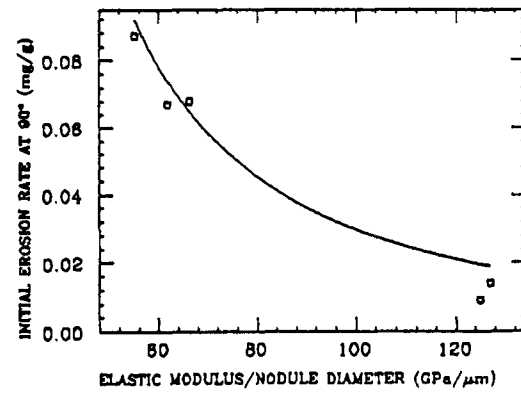## Table 7 Mechanical Properties Obtained from the Nanoindenter

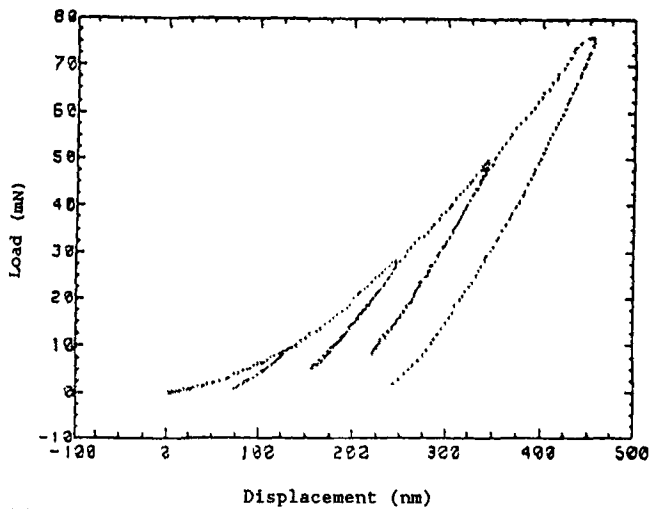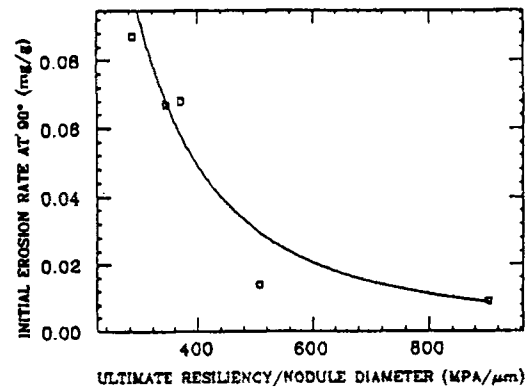| Coating number	Hardness, GPa	Elastic modulus, GPa
1B	36.9	345
2B	32.4	362
3B	30.9	341
4B	43.9	365
5B	31.7	313
6B	36.4	345
7B	31.2	318
8B	24.2	264
9B	33.5	342

(a)

(a)
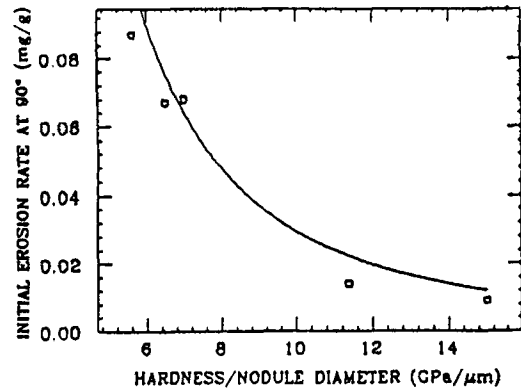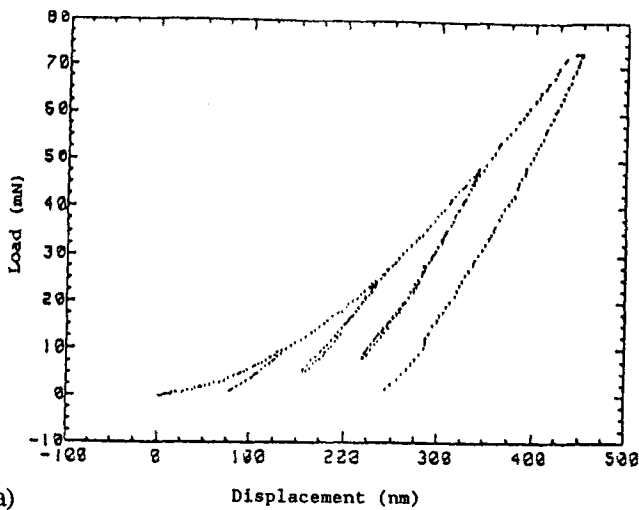
Fig. 16 Load vs displacement curves obtained from the Nanoindenter. (a) Coating 5A and (b) Coating 5B.

(b)

(b)

(c)

Fig. 17 Initial erosion rate at 90° impingement angle as a function of mechanical properties of the coating. (a) Hardness/nodule diameter. (b) Elastic modulus/nodule diameter. (c) Ultimate resiliency/nodule diameter.
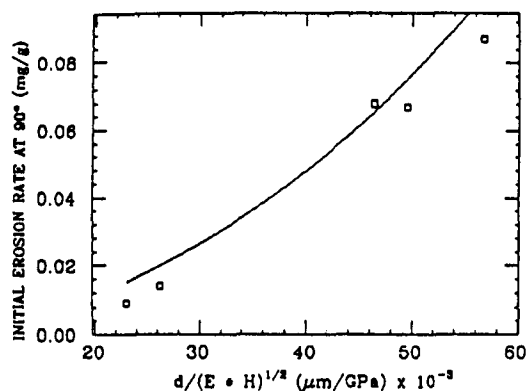
Fig. 18 Initial erosion rate at a 90° impingement angle vs nodule diameter/$(H * E)^{1/2}$.

13). Although this is the mechanism of material removal from a defect-free surface, the presence of craters and kernels rapidly increases the erosion rate by pinhole formation. Because the kernels stand proud on the surface and are poorly bonded to neighboring nodules, they are easily removed during the initial stages of erosion and form pinholes. Because of the brittleness of these coatings, the pinholes enlarge via a chipping mechanism and rapidly expose the substrate to the abrasive stream.

The Group III (i.e., 2 and 4) coatings are particularly resistant to solid particle erosion. These substrates were liquid vapor-honed with 1250-grit Al_2O_3. As a result, they have very smooth surfaces, which promotes the growth of Zone T-type coating morphology. This structure is very dense and relatively defect free. On both macroscopic (Fig. 11) and microscopic scales (Fig. 14), these structures erode in a ductile manner and, hence, are very protective. Indeed, if it were not for the presence of defects, which allows preferential attack, these coatings would not show measurable weight loss except for very long erosion times. Although the presence of defects leads to pinhole formation, Fig. 14 and 15 show that plastic deformation is the dominant erosion mechanism of the pinhole walls. As a result, the pinhole walls are gradually reduced in steepness and are not observed to intersect the coating/substrate interface.

If macroscopic response to an erosive stream at 30 and 90° impingement angles is used as the only predictor of ductile or brittle behavior of a coating, it is possible to reach an erroneous conclusion. For example, the erosion rate for Coating 2A is a maximum at 90° for long exposure times. Although this indicates that the coating is eroding in a brittle manner, microscopic observations of the eroded surface reveals that material removal occurs via a ductile mechanism. The indicated brittle response is attributed to the presence of a high density of kernel and crater defects, which leads to preferential attack and high erosion rates.

According to the data summarized in Table 7, replacement of TiB_2 with 10% WC significantly increased both the hardness and elastic modulus of the coating. The change from a Zone 1 structure to a Zone T-type structure is also reflected in the mechanical properties. The Zone T structure exhibited by sputtered coatings deposited on vapor-honed substrates is very dense and relatively defect free. Therefore, these coatings are somewhat

harder and have higher elastic moduli than those coatings with Zone 1-type microstructures.

The data for the pure TiB_2 coating are especially interesting in that this coating is appreciably softer and has a lower elastic modulus than the same material with 10% Ni present. Transmission microscopy studies[9] have established that sputtered TiB_2 coatings containing 10% Ni are composed of alternating amorphous/polycrystalline bands (see Fig. 8). Energy dispersive analysis of these bands have shown them to be richer in Ni than the bulk and suggests that the Ni is acting as a solid solution strengthener for the crystalline phase. As a consequence, the pure TiB_2 coating exhibits some microscopic ductility, which contributes to its increased erosion resistance.

Comparisons made between erosion rates and the load to cause failure in the scratch test reveal that higher loads must be used to cause failure (4400 to 6500 g) for erosion-resistant coatings than those which perform poorly in erosion testing (2200 to 5300 g). Several variables determine the relative adhesive strength, measured by a scratch test, of a coating/substrate interface. These variables are surface roughness, which is dependent on nodule size and defects present, substrate roughness, chemical compatibility, and residual stress state.

Coatings with large protruding non-close-packed nodules, when scratched by a loaded slider, are more likely to fail than coatings with small nonprotruding close-packed nodules. The poor performance of the large nodule coatings is attributed to fracture and delamination of the coating, which results from interaction of the slider with protruding nodules. When the coating is smoother, the stress concentration resulting from passage of the slider over the surface is diminished. Hence, the larger loads shown in Table 4 are required to cause fracture and delamination of the coating.

Because the coefficients of thermal expansion for the coating and substrate are different, it is expected that a residual stress would develop as the samples cool from the coating temperature. In addition, it is also expected that an intrinsic stress would develop due to an accumulating effect of atomic forces generated throughout the coating volume by atoms that are out of position with respect to the minima in the interatomic force field. Because TiB_2 was deposited at $T/T_m < 0.1$, it is expected that the intrinsic stresses would dominate over the thermal stresses. The coating/substrate interfacial bonds must be able to withstand the shear stresses associated with the intrinsic and thermal stresses. Because the intrinsic stresses increase with increasing coating thickness, it may result in premature interfacial failure and lead to poor adhesion and erosion resistance. Sputter deposited coatings may undergo a transition from compressive to tensile residual stress depending on deposition conditions. The transition has been found to be related to a transition from a Zone T-type growth structure to a Zone 1 structure.

The coatings deposited on Ti-6Al-4V substrates did not perform as well in erosion and scratch tests as those deposited on Inconel 718. This is believed to be due to the differences in the coefficients of thermal expansion of the two substrate materials, because Inconel 718 has a coefficient of thermal expansion nearly double that of Ti-6Al-4V. Therefore, on cooling after sputtering, the coatings applied to Inconel 718 should have much higher compressive stresses compared to coatings applied to Ti-6Al-4V. Because compressive stresses inhibit crack initia-

tion and propagation, they are believed to be responsible for the enhanced performance of Inconel 718 alloy during adhesion and erosion tests compared to the Ti-6Al-4V with the same coatings.

The increased erosion resistance with increasing hardness and elastic modulus is not surprising, because both quantities imply an increase in bond strength. Therefore, more energy must be supplied to the system to remove the coating. The Group I coatings were extremely brittle and failed catastrophically during the early stages of erosion testing. Only those coatings that exhibited ductility on the microscopic scale exhibited significant erosion resistance. Therefore, ductility is an extremely important parameter in determining erosion resistance.

The resiliency of a material is a measure of the amount of energy that can be stored elastically and is given by $\sigma_{ys}^2/2E$, where σ_{ys} is the yield strength. The ultimate resiliency is given by the $\sigma_{uts}^2/2E$, where σ_{uts} is the ultimate tensile strength. Because it was impossible to obtain the ultimate tensile strength for these coatings, the indentation hardness was used to obtain an indication of the ultimate resiliency. The ultimate resiliency is a measure of the amount of energy that a coating can absorb elastically without fracture. As expected (Fig. 17c), the erosion rate of those coatings that exhibited microscopic ductility decreased with increasing resiliency. This also indicates that coatings with high hardnesses and high hardness to elastic modulus ratios should have lower erosion rates.

There have been several attempts to apply indentation fracture mechanics to evaluate the fracture toughness of brittle materials. For example, Lawn et al.[15] have derived an expression from which the fracture toughness, K_{Ic}, may be obtained from microindentation data:

$$K_{Ic} = 0.028 \ c^{3/2}/a^2 \ (HE)^{1/2} \qquad [9]$$

where a is the half diagonal of the indentation, and c is the radial crack size. According to this equation, the fracture toughness is inversely proportional to $(HE)^{1/2}$. As shown in Fig. 18, the data obtained in this investigation indicate that the initial erosion rate of those coatings exhibiting microscopic ductility is inversely proportional to the fracture toughness. This is an expected result and has been documented by others.[2, 14, 16]

5 Conclusion

Examination of nine different coatings has shown that the growth morphology of these coatings is dependent on the substrate preparation. Very smooth substrate surfaces obtained by liquid vapor honing produced coatings with Zone T-type growth morphology, whereas grit-blasted substrates produced coatings with a Zone 1-type morphology. The nodule diameter was also found to be dependent on the substrate preparation.

Due to the large difference in the coefficients of thermal expansion, it is expected that the level of compressive stresses should be much greater in coatings deposited on Inconel 718 compared to Ti-6Al-4V. Therefore, coatings applied to Inconel 718 tend to be more erosion resistant than similar coatings applied to Ti-6Al-4V. Coating properties such as hardness and elastic modulus were found to be independent of the substrate materials used in this investigation. Also, the hardnesses and

elastic moduli of the coatings examined were found to be independent of the nodule diameter.

Coatings deposited on Inconel 718 tend to be more adherent than coatings deposited on Ti-6Al-4V and therefore are more effective barriers to erosion. Defects such as craters and kernels significantly decrease the erosion resistance of those coatings. Also, the erosion resistance of these coatings that exhibit microscopic ductility is dependent on nodule diameter as well as coating properties such as hardness, elastic modulus, and fracture toughness.

In the erosive environments used in this investigation, Zone 1-type coatings fail in a brittle manner. The primary erosion mechanism is chipping and cracking. The Zone T-type coatings generally eroded in a ductile manner, with plastic deformation and plowing being the primary erosion mechanisms. For the same sputtering deposition and substrate parameters, the addition of 10% Ni to TiB_2 significantly degrades the erosion resistance of the coating.

Acknowledgments

References

1. I. Finnie, The Mechanisms of Erosive Wear in Ductile Metals, Corrosion-Erosion Behavior of Materials, K. Nateson, Ed., AIME, 118-126 (1980).

2. A.W. Ruff and S.M. Wiederhorn, Erosion by Solid Particle Impact, Treatise on Materials Science and Technology, C. Preece, Ed., vol. 16, 69-124 (1979).

3. A.G. Evans, M.E. Gulden, and M.E. Rosenblatt, Proc. Royal Soc. London, Ser. A, 361, 343-365 (1978).

4. J.J. Wert and T.N. McKechnie, The Effect of Composition and Process Parameters on the Erosion Resistance of Sputtered Ni-TiB_2 Coatings, Wear, 116, 181-200 (1987).

5. J.J. Wert, D.M. Baker, and T.M. McKechnie, The Effect of Processing Parameters on the Microstructure and Erosion Resistance of $NiCr_3C_2$ Coatings, Surf. Coat. Technol., 33, 245-265 (1987).

6. J.A. Thornton, High Rate Thick Film Growth, Ann. Rev. Mater. Sci., 7, 239 (1977).

7. J.A. Thornton and D.W. Hoffman, Internal Stresses in Titanium, Nickel, Molybdenum and Tantalum Films Deposited by Cylindrical Magnetron Sputtering, J. Vac. Sci. Technol., 14, 164 (1977).

8. K.L. Chopra, Thin Film Phenomena, McGraw-Hill, 295-313 (1969).

9. R.H. Parrish, J.J. Wert, W.C. Oliver, and P.S. Sklad, The Effects of Varying Sputtering Parameters on the Microstructure and Mechanical Properties of 10% Ni + TiB_2 Thin Films, Proc. 7th Int. Conf. Erosion by Liquid and Solid Impact, 18-1 to 18-7 (1987).

10. W.C. Oliver, R. Hutchings, and J.B. Pethica, Measurement of Hardness at Indentation Depths as Low as 20 Nanometers, Microindentation Techniques in Materials Science and Engineer-

ing, P. Blau and B. Lawn, Ed., ASTM Technical Publication 889, 90-108 (1984).

11. M.F. Doerner and W.D. Nix, A Method of Interpreting the Data from Depth-Sensing Indentation Instruments, *J. Mater. Res., 1*, 601-609 (1986).

12. I. Sneddon, The Relation Between Load and Penetration for a Punch of Arbitrary Profile, *Int. J. Eng. Sci., 3*, 47-57 (1965).

13. A.W. Ruff and L.K. Ives, Measurement of Solid Particle Velocity in Erosive Wear, *Wear, 35*, 195-199 (1975).

14. J.A. Thornton, Influence on Apparatus Geometry and Deposition Conditions on the Structure and Topography of Thick Sputtered Coatings, *J. Vac. Sci. Technol., 11*, 666 (1974).

15. B.R. Lawn, A.G. Evans, and D.B. Marshall, Plastic/Elastic Indentation Damage in Ceramics Medial/Radial Cracks System, *J. Am. Ceram. Soc., 63*, 574 (1980).

16. S.M. Weiderhorn and B.J. Hockey, Effect of Material Parameters on the Erosion Resistance of Brittle Materials, *J. Mater. Sci., 18*, 766-780 (1983).